Journal of Alloys and Compounds 622 (2015) 388–393

Contents lists available at ScienceDirect

Journal of Alloys and Compounds

journal homepage: www.elsevier.com/locate/jalcom

First principles study of thermoelectric properties of Li-based half-Heusler alloys

Manoj K. Yadav, Biplab Sanyal *

Department of Physics and Astronomy, Box-516, Uppsala University, 75120, Uppsala, Sweden

ARTICLE INFO

Article history:
Received 10 July 2014
Received in revised form 2 October 2014
Accepted 3 October 2014
Available online 17 October 2014

Keywords:
Thermoelectricity
Seebeck coefficient
Half-Heusler alloys
Density functional theory
Boltzmann transport

ABSTRACT

Thermoelectric materials with good figures of merit are being sought for perpetually. In this paper, thermoelectric properties of LiYZ (Y = Be, Mg, Zn, Cd and Z = N, P, As, Sb, Bi) have been studied employing first principles density functional theory based calculations followed by the solutions of Boltzmann transport equations under relaxation time approximation. Calculated Seebeck coefficients are quite large and are comparable to that of PbTe, a well known thermoelectric material. Doping dependence of the transport coefficients are calculated under rigid band approximation. Except LiZnSb, all the compounds have larger values of power factors for p-type doping than those for n-type doping. The optimal p- and n-type doping levels corresponding to the maximum thermoelectric power factors of these compounds have been calculated, which are important parameters for guiding experimental works.

1. Introduction

The world at present is facing two major problems relating to energy. One is the energy crisis and another is its environmental impact arising from conventional ways of utilizing energy resources. The first problem is driving research for alternative energy resources and the second problem concerns better ways of utilizing the energy resources. Thermoelectricity is considered to be one of the potential ways towards addressing both these problems [1–3]. However, the efficiency of a thermoelectric device is too low to compete with the conventional ways of producing electricity [4,5]. The thermoelectric performance of a thermoelectric material is determined by its figure of merit, ZT given by $ZT = S^2\sigma T/k$, where T is the absolute temperature, S is Seebeck coefficient (also known as thermopower), σ is electrical conductivity and k is the thermal conductivity which is the sum of electronic and lattice contributions to thermal conductivity. With the renewed interest in thermoelectricity, mainly from 1990, the figure of merit has reached above 1 from about 0.5 in 1950 [6]. In order to have larger figure of merit, we need to have a large value for $S^2\sigma$ (also known as power factor) and a small value for thermal conductivity. Though there is no theoretical upper limit for the figure of merit, it is challenging to achieve higher values because of the conflicts between the three transport properties S, σ, k. Thus, a compromise has to be reached among these conflicting parameters to enhance the figure of merit.

Half-Heusler materials are considered to be potential thermoelectric materials [7–9] because of their large temperature stability. Furthermore, they offer the possibility of alloying, which can reduce thermal conductivity due to mass fluctuation [2]. Recently Carrete et al. [10] studied thermal conductivity of a large number of half-Heusler alloys (HHs) from the view point of their thermoelectric prospects. Many HHs have been studied over the years with the main focus on MNiSn (M = Ti, Zr, Hf) [7,9,11]. These HHs have total valence electron count (VEC) equal to 18 in their primitive unit cell. Yang et al. carried out first principles based electronic structure calculations for a large number of HHs having VEC 18 [12]. They further studied thermoelectric properties by calculating thermoelectric transport properties employing Boltzmann transport equations, and found reasonable agreement with experimental results for Seebeck coefficients and the corresponding optimal doping levels. In this paper, we follow a similar approach to investigate the thermoelectric properties of Li-based Nowotny–Juza phase ($X^IY^{II}Z^V$) [13] HHs having VEC = 8 in their primitive cell. There exists reports for the synthesis of some of Li-based $X^IY^{II}Z^V$ HHs [14–16]. There are *ab initio* studies as well with view point of their optoelectronic [18] and piezoelectric [19] prospects, however the study for their thermoelectric properties is lacking.

2. Computational approach

Our calculations involve three main steps: (i) optimization of lattice parameter for each systems, (ii) calculation of band structure , followed by (iii) solution of Boltzmann Transport Equations for calculating thermoelectric properties. The first two sets of cal-

* Corresponding author.
E-mail address: Biplab.Sanyal@physics.uu.se (B. Sanyal).

http://dx.doi.org/10.1016/j.jallcom.2014.10.025
0925-8388/

culations were carried out using the full-potential linearized augmented plane wave (LAPW) method [20] as implemented in the WIEN2k code [21]. The value of $R_{MT}K_{max} = 9$ was chosen for all the calculations, where R_{MT} corresponds to the minimum of the muffin tin radii of the atoms in the unit cell and K_{max} corresponds to the cut-off for the interstitial plane wave part of the basis. The muffin tin radii for Li, Be, N were set to 2.2 a.u. and for Mg, P, Zn, As, Cd, Sb, Bi they were set to 2.5 au. The choice of these radii ensured no charge leakage out of the muffin tins. The lattice parameters were optimized using Perdew–Burke–Ernzerhof (PBE) generalized gradient functional [22] for the approximation of the exchange correlation functional along with $18 \times 18 \times 18$ k-mesh. The band structures were calculated using modified Becke–Johnson (mBJ) potential [23] implemented within WIEN2k along with a finer $34 \times 34 \times 34$ k-mesh. The choice of using mBJ potential was for obtaining correct semiconducting electronic structures. For example, LiCdN and LiCdAs were found to be metallic within PBE approach where as within mBJ approach they are found to be semiconducting.

Using the results from band structure calculations, the transport calculations were performed employing the BoltzTraP [24] code. For the calculation of thermoelectric power factor ($S^2\sigma$), the values for Seebeck coefficient and electrical conductivity are required. The electrical conductivity and the Seebeck coefficient tensors as a function of temperature and the chemical potential can be written as

$$\sigma_{\alpha\beta}(T,\mu) = \frac{1}{\Omega}\int \sigma_{\alpha\beta}(\varepsilon)\left[-\frac{\partial f_o(T,\varepsilon,\mu)}{\partial\varepsilon}\right]d\varepsilon, \quad (1)$$

$$S_{\alpha\beta}(T,\mu) = \frac{1}{eT\Omega\sigma_{\alpha\beta}(T,\mu)}\int \sigma_{\alpha\beta}(\varepsilon)(\varepsilon-\mu)\left[-\frac{\partial f_o(T,\varepsilon,\mu)}{\partial\varepsilon}\right]d\varepsilon, \quad (2)$$

where Ω is the volume of the unit cell, f_o is the Fermi-Dirac distribution function and e is the electronic charge. The kernel of the Eqs. (1) and (2) is the energy projected transport distribution tensor $\sigma_{\alpha\beta}(\varepsilon)$, which contains the system dependent information, and can be expressed as

$$\sigma_{\alpha\beta}(\varepsilon) = \frac{e^2}{N}\sum_{i,\mathbf{k}}\tau_{i,\mathbf{k}}v_\alpha(i,\mathbf{k})v_\beta(i,\mathbf{k})\frac{\delta(\varepsilon-\varepsilon_{i,\mathbf{k}})}{d\varepsilon}, \quad (3)$$

where N is the number of k-points, i is the band index, $\mathbf{k}$ is the wave vector and $v_\alpha(i,\mathbf{k})$ is the group velocity, which can be obtained from the band structure calculations as

$$v_\alpha(i,\mathbf{k}) = \frac{1}{\hbar}\frac{\partial\varepsilon_{i,\mathbf{k}}}{\partial k_\alpha}, \quad (4)$$

where $\hbar$ is the reduced Planck constant.

The wave vector dependent relaxation time appearing in the expression for transport distribution tensor (Eq. (3)) is difficult to be determined from first principles calculations and hence Eq. (3) is solved under constant relaxation time approximation (RTA) [25]. The RTA is based on the assumption that the relaxation time does not vary strongly with energy on the scale of k_BT, where k_B is the Boltzmann constant. In fact the calculation of transport coefficients involves the derivative of Fermi function whose magnitude varies significantly within a small energy window about $10k_BT$ (0.26 eV for $T = 300$ K) near the chemical potential, and τ is assumed to remain nearly constant within this small energy range. Thus, it turns out to be a reasonably good approximation and has been able to successfully describe the transport coefficients of many materials [24,26–28]. Within RTA, the Seebeck coefficient can be calculated without any adjustable parameter. However, the electrical conductivity has to be calculated with respect to the relaxation time and hence instead of calculating the absolute power factor $S^2\sigma$, we calculate the power factor with respect to relaxation time ($S^2\sigma/\tau$). This is a reasonable approach for studying qualitative trend of thermoelectric properties of a particular class of materials.

3. Result and discussions

A typical crystal structure of a Nowotny–Juza phase half-Heusler compound with common formula XYZ is shown in Fig. 1. The crystal structure corresponds to MgAgAs type structure with space group $F\bar{4}3m$ (space gr. no. 216). The structure can be assumed to be derived from the combination of a rock-salt type (NaCl) structure with a zinc-blende type structure. The most electropositive element X (Li in our case) and the element with intermediate electronegativity Y (Be, Mg, Zn, Cd) build the rock-salt type structure. The zinc-blende type structure is built from the most electronegative element Z (N, P, As, Sb, Bi) and the element with the intermediate electronegativity Y. Thus, the Wyckoff positions for X, Y and Z are 4b(0.5, 0.5, 0.5), 4a(0, 0, 0) and 4c(0.25, 0.25, 0.25) respectively. Thomas [29] has carried out extensive *ab initio* studies for the crystal structures of various types of HHs and has found the aforementioned structure to be the most favorable for the Nowotny–Juza phase (I–II–V) HHs.

Now we present and analyze the results of electronic structure calculations and then we will discuss the transport properties relating thermoelectric performance. The calculated lattice parameters obtained using PBE-GGA functional and band gaps using TB-mBJ potential along with the corresponding available experimental values are listed in Table 1. As can be seen in Table 1, the optimized lattice parameters agree very well with the available experimental lattice parameters for LiMgZ [30,32], LiZnZ [33–35] and LiCdZ [14] except for the case of LiCdAs where our calculated value is about 2% larger than the experimental value [36]. Unlike general underestimation of band gaps due to the well known limitation of ground state density functional theory using local or semilocal approximations, our calculated band gaps under TB-mBJ approach are closer to the available experimental values. In fact we find some overestimated values in the cases of LiMgN, LiZnP, LiZnAs and highly overestimated band gap for LiCdP. However, our calculated lattice parameters (including the case of LiCdAs) as well as band gaps agree very well with previous calculations [18]. Except LiZnBi and LiCdBi, all the alloys show insulating behavior within TB-mBJ approach. LiZnBi and LiCdBi show metallic behaviour, which could not be further confirmed as there is no any literature report for these two alloys. Since metallic systems are not good for thermoelectric prospects mainly because they cannot maintain thermal gradient, we exclude these two compounds from study of thermoelectric properties. The band gaps of other remaining alloys range from as low as 0.21 eV (for LiCdN) to relatively high value of 4.23 eV (for LiBeN).

Fig. 2 shows the plot for density of states (DOS) for some selected HHs. The dominant states at valence band maxima (VBM) of these HHs come from atoms at Z positions, and the analysis of orbital projected DOS (not shown in Fig. 2 for the sake of clarity) reveals that these are p-states of Z. The dominant states at conduction band minima (CBM) are the strongly s–p hybridized states coming from s orbital of Y and p orbital of Z along with a small contribution from Li-s states. Similar composition of DOS at band edges is found for all the remaining HHs. If we analyze the variation of band gap (see Table 1), we find with few exceptions the variation of band gaps follow two kinds of general trends: (i) with XY fixed the band gap decreases with increasing atomic number of Z and (ii) with XZ fixed the band gap decreases with increasing atomic number of Y. In either case there is increase in average atomic number, $\langle\mathcal{Z}\rangle$ in XYZ, and hence the band gap decreases linearly with the increasing average atomic number, $\langle\mathcal{Z}\rangle = 1/N\sum_i^N \mathcal{Z}_i$, where N is the number of atoms in the unit cell.

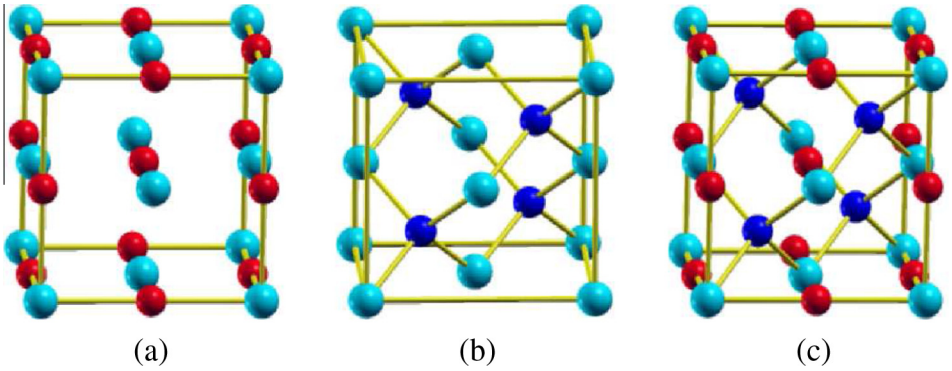

Fig. 1. (a) Rock-salt structure, (b) zinc-blende structure and (c) half-Heusler structure. X, Y and Z atoms are shown as red, turquoise and blue balls respectively. (For interpretation of the references to colour in this figure legend, the reader is referred to the web version of this article.)

Table 1
Calculated lattice parameters (Å) using PBE-GGA approach and band gaps (eV) obtained using TB-mBJ potential along with the available experimental values.

	Lattice constants		Band gaps	
	This work	Experiment	This work	Experiment
LiBeN	4.38		4.23	
LiBeP	5.38		1.77	
LiBeAs	5.59		1.60	
LiBeSb	6.05		1.30	
LiBeBi	6.23		1.06	
LiMgN	5.01	4.96[a]	3.65	3.23[i]
LiMgP	6.02	6.00[b]	2.26	2.43[b]
LiMgAs	6.20	6.18[b]	1.60	2.38[j]
LiMgSb	6.63		1.73	
LiMgBi	6.76	6.74[c]	1.24	
LiZnN	4.93	4.91[d]	1.70	1.91[d]
LiZnP	5.77	5.76[e]	2.20	2.04[e]
LiZnAs	5.99	5.94[f]	1.53	1.51[f]
LiZnSb	6.41		1.42	
LiZnBi	6.62		Metallic	
LiCdN	5.38		0.21	
LiCdP	6.14	6.10[g]	1.47	0.85[k]
LiCdAs	6.35	6.23[h]	0.77	
LiCdSb	6.74		0.90	
LiCdBi	6.93		Metallic	

[a] Ref. [32].
[b] Ref. [30].
[c] Ref. [31].
[d] Ref. [35].
[e] Ref. [34].
[f] Ref. [33].
[g] Ref. [14].
[h] Ref. [36].
[i] Ref. [16].
[j] Ref. [19].
[k] Ref. [17].

This result is consistent with earlier studies of Nowotny–Juza phase HHs [18,37].

Next we move on to study thermoelectric properties. Under rigid band approximation, the Fermi level moves up or down depending on doping type, but the underlying band structure is not allowed to change. Thus, only one band structure calculation is required for calculating transport properties at various doping levels. The approach is helpful for band structure based theoretical investigation for thermoelectric performance of a material, and has been widely used [27,38,24]. The variation of transport properties with the varying Fermi level (μ) for LiYAs (Y = Be, Mg, Zn, Cd) is plotted in Fig. 3. Since LiYAs lies in the middle of each of the four LiYZ groups studied in this paper so we chose LiYAs for this representative plot. In general, as the Fermi level moves towards the band edges the density of states at the Fermi level increases. However, the Seebeck coefficient rapidly decreases as the Fermi level leaves the band gap and enters the band edges. In all the cases very high values for Seebeck coefficients are found away from the band edges towards the middle of the gap, however for better thermoelectric performance the value of Seebeck coefficient just inside band edge is important. Thus, for a better thermoelectric performance it is important that the material retains substantial value of Seebeck coefficient when the Fermi level enters the band edge.

The thermoelectric power factors in all these cases is larger for p-type doping (corresponding to negative values of μ) than those for n-type doping (corresponding to positive values of μ). Among the four LiYAs, LiMgAs has the maximum power factor. It also has the largest value of DOS corresponding to its maximum power factor. The large DOS at Fermi level indicates larger electrical conductivity which contributes in enhancing the power factor. Furthermore, LiMgAs has the largest value for the Seebeck coefficient which is another factor responsible for the large power factor. The remaining three HHs have more or less comparable values for DOS

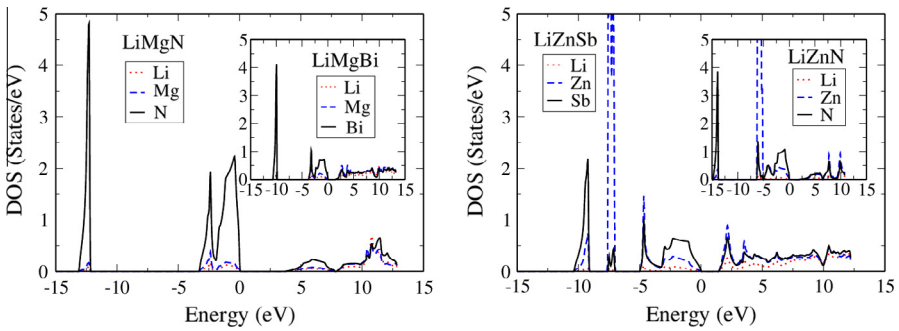

Fig. 2. DOS plot for (left) LiMgN and LiMgBi (inset) and (right) LiZnSb and LiZnN (inset).

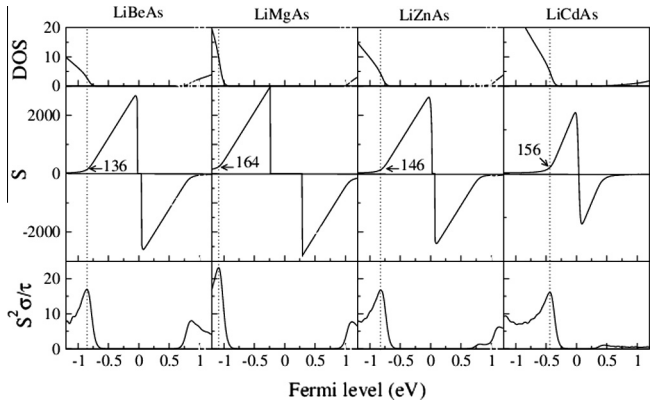

Fig. 3. Density of states and thermoelectric transport properties versus Fermi levels at 300 K. The units of DOS, Seebeck coefficients and thermoelectric power factors are states eV^{-1} u c^{-1}, $\mu V\,K^{-1}$ and $10^{14}\,\mu W\,cm^{-1}\,K^{-2}\,s^{-1}$ respectively. The dotted vertical lines are drawn passing through the peak value of thermoelectric power factors and the corresponding values of Seebeck coefficients are shown by arrows. The Fermi level of 0 eV corresponds to the middle of the band gap in each case and hence −ve and +ve values of μ correspond to p-type and n-type doping respectively.

Table 2
Optimal doping levels (carrier/u.c.) and corresponding values for thermoelectric power factors with respect to relaxation time, $S^2\sigma/\tau$ (10^{14} μW/cm K^2 s) for both p- and n-type dopings. Power factors with values below 5 are indicated by /.

	p-Type doping		n-Type doping	
	Doping level	Power factor	Doping level	Power factor
LiBeN	0.009	25.35	0.002	8.27
LiBeP	0.005	17.85	0.002	8.22
LiBeAs	0.005	16.94	0.003	8.02
LiBeSb	0.004	15.02	0.003	8.28
LiBeBi	0.004	14.17	0.004	8.32
LiMgN	0.038	37.73	0.016	7.26
LiMgP	0.020	24.63	0.003	7.93
LiMgAs	0.017	23.15	0.004	7.71
LiMgSb	0.015	20.27	0.004	7.60
LiMgBi	0.012	19.38	0.015	6.27
LiZnN	0.012	20.92	/	/
LiZnP	0.008	17.20	0.003	8.16
LiZnAs	0.008	16.76	/	/
LiZnSb	0.006	15.61	0.066	38.46
LiCdN	0.016	19.19	/	/
LiCdP	0.008	16.71	/	/
LiCdAs	0.009	16.12	/	/
LiCdSb	0.008	15.04	/	/

and Seebeck coefficients and consequently they have more or less similar values for power factors. In order to achieve ZT∼1, the material must have minimum value of Seebeck coefficient, $S \sim 150\,\mu V/K$ [2], and all these alloys seem to fulfill this requirement. In fact these HHs have Seebeck coefficients comparable to that of the well known thermoelectric material PbTe. The Seebeck coefficient of PbTe calculated with the similar approach is below 150 μV/K within the concentration range of 10^{19}–10^{20}/cm^3 at 300 K [39].

One of the important aspects of theoretical investigation for thermoelectric material is to find the optimal doping level at which the thermoelectric power factor attains the maximum value. The theoretical optimal doping level provides guideline in narrowing down doping window in experiments. To serve the purpose of finding optimal doping levels, we calculated Seebeck coefficients and electrical conductivity with respect to relaxation time (σ/τ) at various doping concentrations ranging from 10^{19} to 10^{22}/cm^3 for both p- and n-type dopings. The resulting power factor with respect to the relaxation time ($S^2\sigma/\tau$) was then plotted against carrier concentration and the optimal doping level was noted corresponding to the peak value of power factor in each case. A representative plot for variation of power factor with carrier concentration for each type of doping is shown in Fig. 4(a). The results for maximum power factors and corresponding optimal doping levels for all the alloys are tabulated in Table 2. It is clear that except LiZnSb, all HHs have larger values of power factors for p-type doping than those for n-type doping.

One of the criteria for large power factor is that the material must have a high DOS at the band edge [26,40]. The VBM of LiMgN has the presence of large DOS compared to LiMgBi (Fig. 2) and hence LiMgN has a large power factor for p-type doping. Furthermore, the very low DOS at the CBM of LiMgN is the reason for its low power factor for n-type doping. On the similar ground we can infer that LiZnSb should have a large power factor for n-type doping than for p-type doping as it has large DOS at CBM compared to VBM. Again, the comparison of DOS at CBM of LiZnSb and LiZnN clearly evidences the reason for low power factor for LiZnN for n-type doping. The maximum power factor for p-type doping is obtained for LiMgN while for the n-type doping LiZnSb shows the maximum power factor. Assuming the relaxation time to be $\sim 10^{-14}$ s, the power factor of n-type LiZnSb (38.46 μW/cm K^2 s) turns out to be comparable to that of n-type PbTe (35 μW/cm K^2 s) at 300 K [41]. Overall a general trend for the

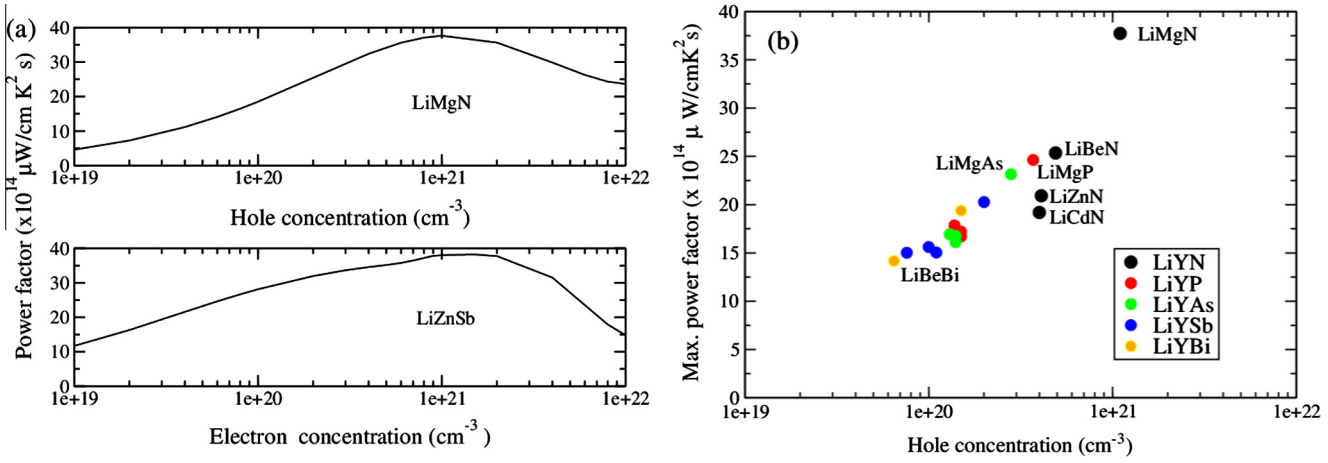

Fig. 4. (a) Variation of thermoelectric power factors of LiMgN and LiZnSb with carrier concentration, (b) peak values of thermoelectric power factors of HHs plotted against optimum doping levels.

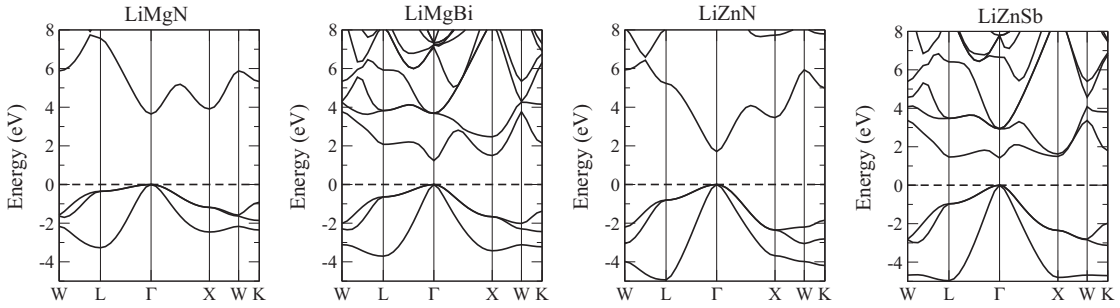

Fig. 5. Band structures for selected HHs along selected symmetry directions. The energy axis in each case is plotted with respect to the VBM.

decrease of power factor is seen when we vary Z from N to Bi with X and Y fixed. Most of high power factors for p-type doping correspond to doping concentration within the range of 1.0×10^{20}–$1.0 \times 10^{21}/cm^3$, as can be seen in Fig. 4(b). The RBA is questionable for heavy doping where the Fermi level lies deep inside the band. Fortunately, in all our cases, the doping is mild. Even for the heaviest doping (n-type LiZnSb), the Fermi level is only 0.35 eV above the CBM.

Finally we analyze the reason for large power factors for LiMgN and LiZnSb on the basis of their band structures. We compare the band structure of LiMgN with that of LiMgBi, which has the lowest power factor among LiMgZ for p-type doping. If we look at the VBM of their band structure plots (Fig. 5), we find that VBM of LiMgN between L and Γ is flatter than the corresponding VBM of LiMgBi. The flat band at VBM of LiMgN is resulting from the rapidly varying DOS at VBM (Fig. 2). The flatter band implies heavy effective mass, which enhances the Seebeck coefficient and hence also the thermoelectric power factor. The largest effective mass at the Γ point of VBM of LiMgN (Table 3) clearly supports its largest value of thermoelectric power factor. Moreover, the general trend of decreasing thermoelectric power factor on going from LiYN to LiYBi also follows the trend of decreasing effective mass at VBM on going from LiYN to LiYBi. The VBM-1 band, which is degenerate with VBM at Γ point have lighter effective masses. Thus, the VBM have a combination of heavier and lighter holes which is good for thermoelectric performance [3,39,42]. The heavier holes contribute to enhance Seebeck coefficient where as the lighter holes being highly mobile contribute to enhance conductivity and hence the combination of lighter and heavier holes enhances thermoelectric power factor. All LiYN compounds have relatively larger rapidly varying DOS at VBM compared to those of other LiYZ and hence they have relatively large values for power factors.

Next, we compare the CBM of LiZnSb with that of LiZnN, which has the lowest power factor among LiZnZ for n-type doping. Again, a more non-dispersive and non-parabolic CBM along L–Γ and Γ–X directions for LiZnSb compared to that of LiZnN (Fig. 5) clearly indicates a large power factor for LiZnSb for n-type doping. However, large values for effective masses at CBM of LiBeSb and LiBeBi (Table 3) also indicates the possibility for their large thermoelectric power factor for n-type doping, but in fact they have lower values for the thermoelectric power factor. This can be explained on the basis of spread of CBM band structures. Their lowest CBM lies only at X point unlike in the case of LiZnSb which has nearly degenerate CBM at L, Γ and X points. Thus, in the case of LiZnSb heavier electrons from X and L pockets and lighter ones from Γ pocket together contribute to enhance its thermoelectric power factor. Similar argument has been put forward by Lee et al. for larger thermopower in hole doped HfCoSb and ZrCoSb over HfIrSb and ZrIrSb [43]. Moreover, LiZnSb has one more higher conduction band CBM+1, which is degenerate with CBM at X point. This band contributes lighter electrons and thus further providing better combination of heavy and light electrons at CBM.

Table 3
The calculated effective masses (m^*/m_e) using the curvature of the band structures. Two values are calculated along different directions about the specified k points.

	p-Type doping		n-Type doping			
k Point	Γ		X		Γ	L
Band	VBM	VBM − 1	CBM	CBM+1	CBM	CBM
LiBeN	5.7, 2.7	0.9, 1.6	0.8, 0.5			
LiBeP	3.2, 1.6	0.6, 0.9	0.9, 0.4			
LiBeAs	2.8, 1.5	0.5, 0.8	1.0, 0.3			
LiBeSb	2.0, 1.3	0.5, 0.7	2.4, 0.3			
LiBeBi	1.5, 1.2	0.6, 0.7	1.7, 0.3			
LiMgN	9.9, 4.0	1.0, 1.7		1.0, 0.7		
LiMgP	4.8, 2.3	0.6, 1.0	0.8, 0.4			
LiMgAs	4.5, 2.2	1.4, 1.0	0.7, 0.4			
LiMgSb	3.4, 1.7	0.6, 0.8	0.6, 0.3			
LiMgBi	3.2, 1.6	0.5, 0.8		0.3, 0.3		
LiZnN	4.6, 2.1	0.8, 1.4		1.0, 0.7		
LiZnP	3.0, 1.6	0.6, 0.8	1.0, 0.4			
LiZnAs	2.7, 1.2	0.5, 0.7		0.4, 0.4		
LiZnSb	2.2, 1.2	0.5, 0.6	2.6, 0.4	0.8, 0.3	0.4, 0.3	3.3, 0.9
LiCdN	4.5, 2.1	0.8, 1.4		0.9, 0.7		
LiCdP	2.8, 1.5	0.6, 0.8		0.6, 0.5		
LiCdAs	2.7, 1.4	0.5, 0.7		0.4, 0.4		
LiCdSb	2.4, 1.3	0.4, 0.6		0.3, 0.2		

4. Summary

Our density functional calculations reveal that despite being relatively large band gap materials, the Li-based Nowotny–Juza phase materials have large values of Seebeck coefficients and thermoelectric power factors, which are comparable to those of the well known thermoelectric material PbTe. Both the presence of large DOS and rapidly varying DOS at VBM mainly coming from p-states of Z (N, P, As, Sb and Bi), have been found responsible for large power factors for p-type doped cases. The large n-type power factor in LiZnSb is due to the presence of highly spiky DOS at CBM, coming from the s–p hybridized states of Sb and Zn. The optimal doping levels corresponding to the maximum power factors for both p- and n-type dopings have been calculated. We hope that our theoretical predictions will motivate experimental studies on these systems.

Acknowledgements

MKY acknowledges financial support from Erasmus Mundus-EXPERTS III program. BS acknowledges Swedish National Infrastructure for Computing (SNIC) for the allocation of supercomputing time.

References

[1] G.J. Snyder, E.S. Toberer, Nat. Mater. 7 (2008) 105.
[2] H. Alam, S. Ramakrishna, Nano Energy 2 (2013) 190.
[3] M.K. Yadav, B. Sanyal, Mater. Res. Express 1 (2014) 015708.
[4] S.K. Yee, S. LeBlanc, K.E. Goodson, C. Dames, Energy Environ. Sci 6 (2013) 2561.
[5] G.B. Vining, Nat. Mater. 8 (2009) 83.
[6] C. Zhi-Gang, H. Guang, Y. Lei, L. Cheng, J. Zou, Prog. Mater. Sci.: Mater. Int. 22 (2012) 535.
[7] H. Hohl, A.P. Ramirez, C. Goldmann, G. Ernst, B. Wlfing, E. Bucher, J. Phys. Condens. Matter 11 (1999) 1697.
[8] G.S. Nolas, J. Poon, M. Kanatzidis, MRS Bull. 31 (2006) 199.
[9] C. Yu, T.-J. Zhu, R.-Z. Shi, Y. Zhang, X.-B. Zhao, J. He, Acta Mater. 57 (2009) 2757.
[10] J. Carrete, W. Li, N. Mingo, Phys. Rev. X 4 (2014) 011019.
[11] C. Uher, J. Yang, S. Hu, D.T. Morelli, G.P. Meisner, Phys. Rev. B 59 (1999) 8615.
[12] J. Yang, H. Li, T. Wu, W. Zhang, L. Chen, J. Yang, Adv. Funct. Mater. 18 (2008) 2880.
[13] H. Nowotny, K. Bachmayer, Monatsch. Chem. 81 (1950) 488.
[14] R. Bacewicz, T.F. Ciszek, Appl. Phys. Lett. 52 (1988) 1150.
[15] A. Beleanu, M. Mondeshki, Q. Juan, F. Casper, C. Felser, F. Porcher, J. Phys. D: Appl. Phys. 44 (2011) 475302.
[16] K. Kuriyama, K. Nagasawa, K. Kushida, J. Cryst. Growth 237–239 (2002) 2019.
[17] C. Kandpal, C. Felser, R. Seshadri, J. Phys. D 39 (2006) 776.
[18] S. Kacimi, H. Mehnane, A. Zaoui, J. Alloys Comp. 587 (2014) 451.
[19] A. Roy, J.W. Bennett, K.M. Rabe, D. Vanderbilt, Phys. Rev. Lett. 109 (2012) 037602.
[20] D.J. Singh, L. Nordstrom, Planewaves, Pseudopotentials and the LAPW Method, second ed., Springer, Berlin, 2006.
[21] P.Blaha, K. Schwarz, G.K.H. Madsen, D. Kvasnicka and J. Luitz, WIEN2k, An Augmented Plane Wave + Local Orbitals Program for Calculating Crystal Properties, Karlheinz Schwarz Technical University, Wien, 2001.
[22] J.P. Perdew, K. Burke, M. Ernzerhof, Phys. Rev. Lett. 77 (1996) 3865.
[23] F. Tran, P. Blaha, Phys. Rev. Lett. 102 (2009) 226401.
[24] G.K.H. Madsen, D.J. Singh, Comput. Phys. Commun. 175 (2006) 67.
[25] H. Gzyl, J. Stat. Phys. 29 (1982) 617.
[26] X. Chen, D. Parker, M. Du, D.J. Singh, New J. Phys. 15 (2013) 043029.
[27] G.K.H. Madsen, J. Am. Chem. Soc. 128 (2006) 12140.
[28] T.J. Scheidemantel, D. Ambrosch, T. Thounhauser, J.V. Bading, J.O. Sofo, Phys. Rev. B 68 (2003) 125210.
[29] G. Thomas, Phys. Rev. B 82 (2010) 125210.
[30] K. Kuriyama, K. Kushida, R. Taguchi, Solid State Commun. 108 (1998) 429.
[31] A. Belsky, M. Hellenbrandt, V.L. Karen, P. Luksch, Acta Crystallogr. Sect. B 58 (2002) 364.
[32] K. Kuriyama, R. Taguchi, K. Kushida, K. Ushiyama, J. Cryst. Growth 802 (1999) 198.
[33] K. Kuriyama, T. Kato, K. Kawada, Phys. Rev. B 49 (1994) 11452.
[34] K. Kuriyama, T. Kato, Phys. Rev. B 37 (1988) 7140.
[35] K. Kuriyama, T. Kato, T. Tanaka, Phys. Rev. B 49 (1994) 4511.
[36] R. Bacewicz, T.F. Ciszek, Mater. Res. Bull. 23 (1988) 1247.
[37] F. Casper, T. Graf, S. Chadov, B. Balke, C. Felser, Semicond. Sci. Technol. 27 (2012) 063001.
[38] L. Chaput, P. Pecheur, J. Tobola, H. Scherrer, Phys. Rev. B 72 (2005) 085126.
[39] D.J. Singh, Phys. Rev. B 81 (2010) 195217.
[40] L. Zhang, M. Du, D.J. Singh, Phys. Rev. B 81 (2010) 075117.
[41] B. Je-Hyeong, B. Zhixi, S. Ali, Phy. Rev. B 87 (2013) 075204.
[42] D. Parker, D.J. Singh, Phys. Rev. B 85 (2012) 125209.
[43] M. Lee, F.P. Poudeu, S.D. Mahanti, Phy. Rev. B 83 (2011) 085204.